Supplementary Information

Oligo(ethylene glycol)-modified benzotriazole-based ultra-narrow bandgap acceptor for efficient transparent organic photovoltaic

Zibo Zhou[1,2,‡], *Yibin Zhou*[2,3,‡], *Dianyi Liu*[1,2,3,4 *]

[1] Zhejiang University, Hangzhou, Zhejiang 310027, China.

[2] Zhejiang Key Laboratory of 3D Micro/Nano Fabrication and Characterization, School of Engineering, Westlake University, Hangzhou, Zhejiang 310030, China.

[3] Institute of Advanced Technology, Westlake Institute for Advanced Study, Hangzhou, Zhejiang 310024, China.

[4] Westlake Optoelectronic Technology Co., Ltd., Hangzhou, Zhejiang 310024, China.

[‡] These authors contributed equally to this work.

Corresponding Author

* Email: liudianyi@westlake.edu.cn

1. Materials and Methods

Materials

PTB7-Th was purchased from Nanjing Zhiyan Technology Co., Ltd. PEDOT:PSS (Clevios P VP.Al 4083) was supplied by Heraeus. PDINN was obtained from Organtec Ltd. Phenanthrene (PAT) was purchased from Bide Pharmatech Ltd. ZnO nanoparticles was prepared based on our reported literature.[1] Silver nanowires ink dispersion was supplied from Zhejiang Kechuang Advanced Materials Technology Co. Ltd. Unless otherwise stated, all the other chemicals and solvents were obtained from and used as received without further purification. ^{1}H and ^{13}C NMR spectra were obtained with a Bruker AV-500/600 MHz NMR spectrometer. Mass spectra were collected on AXIMA-Performance from SHIMADZU Corporation using dithranol as matrix.

Device fabrication

Opaque device fabrications.

A typical opaque device was fabricated on ITO substrate with the conventional structure of Glass/ITO/PEDOT:PSS/active layer/PDINN/Ag. ITO substrates were precleaned using consecutive ultrasonic baths in deionized water and ethanol, followed by plasma treatment for 2 minutes. Subsequently, PEDOT:PSS (diluted to 50% by deionized water for use) was spin-coated on the ITO substrate at 4000 rpm for 30 seconds and then annealed at 150 °C for 2 minutes. PTB7-Th:BZ-OEG (D/A=1:1.7) and PTB7-Th:BZ-OEG:PA-2Br (D/A=1:1.2:0.5) were dissolved in *o*-Xylene at the donor concentration of 7.4 mg mL^{-1}. For the fabrication of optimal devices, the weight ratio of PAT to acceptors was 70% as the additive to prepare active layer solutions. These solutions were stirred at 60 °C for 4 hours, and the substrates were preheated on a hotplate to 100 °C for 10 minutes before the active layer deposition. Then, active layer solutions were immediately spin-coated on the PEDOT:PSS layer at 2500 rpm for 60 seconds, followed by annealing at 100 °C for 5 minutes. Subsequently, a solution of PDINN dissolved in methanol at a concentration of 1 mg mL^{-1} was spin-coated on the

active layer at 4000 rpm for 30 seconds. Finally, 100 nm Ag back electrode was deposited on the PDINN layer via thermal vacuum evaporation. The actual active area was defined by a 3 mm^2 mask.

Transparent device fabrications.

A typical transparent device was fabricated on ITO substrate with the conventional structure of Glass/ITO/PEDOT:PSS/active layer/ZnO NPs/AgNWs. ITO substrates were precleaned using consecutive ultrasonic baths in deionized water and ethanol, followed by plasma treatment for 2 minutes. Subsequently, PEDOT:PSS (diluted to 50% by deionized water for use) was spin-coated on the ITO substrate at 4000 rpm for 30 seconds and then annealed at 150 °C for 2 minutes. PTB7-Th:BZ-OEG:PA-2Br (D/A=1:1.2:0.5) was dissolved in *o*-Xylene at the donor concentration of 5.2 mg mL^{-1}. The weight ratio of PAT to acceptors was 70% as the additive to prepare active layer solutions. These solutions were stirred at 60 ℃ for 4 hours, and the substrates were preheated on a hotplate to 100 ℃ for 10 minutes before the active layer deposition. Then, active layer solutions were immediately spin-coated on the PEDOT:PSS layer, followed by annealing at 100 °C for 5 minutes. To ultimately prepare TOPVs with the AVT of ~70%, the active layer thicknesses was controlled at ~55 nm. Then, ZnO NPs was spin-coated on the active layer at 4000 rpm for 2 minutes. Finally, silver nanowires ink (AgNWs suspension) was deposited on the ZnO layer at a spin speed of 2500 rpm for 2 minutes. The actual active area was defined by a 3 mm^2 mask.

Characterization Methods

UV-vis absorption

Solution absorption spectra of acceptors were monitored by a JASCO V-770 spectrometer.

UV-vis-NIR absorption (A), transmission (T) and reflection (R) spectra of films and devices were measured using Cary 6000i as a spectrophotometer with a bandwidth of ≈ 2 mm under ambient conditions.

Photoluminescence (PL)

Fluorescence spectra of BZ-OEG was determined by FLS1000 Edinburgh instruments. BZ-OEG film was spin-coated on glass substrate at a spin speed of 2000 rpm for 60 seconds. The excitation wavelength and bandwidth were set as 800 nm and 10 nm with a scan range from 820 to 1580 nm.

Cyclic voltammetry (CV)

Cyclic voltammetry (CV) was done on a CHI600A electrochemical workstation by utilizing the acetonitrile solution of 0.1 mol L^{-1} tetrabutylammonium-hexafluorophosphate (Bu_4NPF_6). The CV curves were recorded versus the potential of $Ag/AgNO_3$ reference electrode, which was calibrated by the ferrocene-ferrocenium (F_C/F_C^+) redox couple (4.8 eV below the vacuum level). Then LUMO and HOMO levels were calculated by the equation of $E_{LUMO/HOMO} = -e\,(E_{red/ox}+4.8)$ (eV).

Space-charge-limited current measurement (SCLC)

The charge carrier mobilities of PTB7-Th:PA-2X blends were measured by fitting the dark currents with a diode configuration of Glass/ITO/PEDOT:PSS/active layer/ MoO_3/Ag for the hole-mobility and Glass/ITO/ZnO NPs/active layer/PDINN/Ag for the electron-mobility devices. The hole and electron mobilities were calculated according to the Mott–Gurney law described as:

$$J = 9\varepsilon_0\varepsilon_r\mu V^2/8L^3$$

where J is the current density, ε_0 is the permittivity of free space, ε_r is the permittivity of the organic materials, μ is the charge carrier mobility, V is the effective voltage and L is the film thickness of active layer.

Fourier transform photocurrent spectrometer EQE (FTPS-EQE) and Electroluminescence (EL) measurements

To investigate energy loss pathways in OPVs, Fourier transform photocurrent spectrometer EQE (FTPS-EQE) measurements were conducted using an integrated characterization platform (QE-RX, Enlitech). Electroluminescence (EL) spectra and the corresponding EQE_{EL} values were obtained by biasing the OPVs with external voltage and current sources (LQ-50X, Enlitech).

The energy losses (E_{loss}) can be evaluated through the following equation:

$$E_{loss} = EPV\ g - qV_{OC} = \Delta E_1 + \Delta E_2 + \Delta E_3$$

where $EPV\ g$ denotes the optical bandgap of the active layer, ΔE_1 represents the radiative recombination loss beyond $EPV\ g$, ΔE_2 quantifies the radiative recombination loss under $EPV\ g$, and ΔE_3 corresponds to the non-radiative recombination loss.

The ΔE_3 can be obtained from the following equation:

$$\Delta E_3 = -kTln(EQE_{EL})$$

This methodology provides a comprehensive framework for quantifying individual contributions to energy loss in OPVs, facilitating the identification of loss mechanisms that limit overall device performance.

Meanwhile, the Urbach energy (E_u) is analyzed according to the reported literatures.[2]

The abovementioned measurement and derived analysis are performed by Zhengzhou Testing Family of Master and Doctor Technology Co., LTD, China.

Atomic force microscope (AFM)

Surface topographies of active layers were performed by Atomic Force Microscope in tapping mode (Bruker Dimension® Icon™).

Transmission electron microscope (TEM)

The microphase morphology of active layer films was characterized using a TEM at an accelerating voltage of 120 kV. The active layer solutions were spin-coated onto a Glass/PEDOT:PSS substrate. Then, the films were floated on water, transferred onto a copper grid, and naturally dried to complete sample preparation.

Grazing-incidence wide-angle X-ray scattering (GIWAXS)

Grazing-incidence wide-angle X-ray scattering (GIWAXS) measurements were performed by Bruker D8 Venture & Bruker Nanostar using a Cu X-ray source (8.04 keV, 1.54 Å) with a PHOTON III CAPD detector.

PTB7-Th:BZ-OEG (D/A=1:1.7) and PTB7-Th:BZ-OEG:PA-2Br (D/A=1:1.2:0.5), were dissolved in *o*-Xylene at the donor concentration of 7.4 mg mL^{-1}. These solutions were spin-coated on the precleaned Si wafer in the glovebox. After spin-coating, the pristine films were annealed at 100 ℃ for 5 minutes for further measurements.

Contact angles measurements

Miscibility properties of active layer materials were characterized by Dataphysics-OCA20. The water and ethylene glycol contact angles of PTB7-Th, BZ-OEG, and PA-2Br were measured on the surfaces of their neat films. The surface tensions (γ) of these films were obtained according to OWRK model, and the Flory-Huggins interaction parameters (χ) were calculated to assess miscibility of binary blends from the following equation:

$$\chi_{1,2} = k(\sqrt{\gamma_1} - \sqrt{\gamma_2})^2$$

where γ is the surface tension of the material, k is the proportionality constant.

Transient absorption spectroscopy (TAS)

The femtosecond transient absorption measurements were carried out using a Yb: KGW regenerative amplified femtosecond laser system (Light Conversion, 1027 nm, 190 fs, 200 μJ/pulse, and 100 kHz repetition rate) and a Femto-TA100 spectrometer (Time-Tech Spectra LLC).

Photovoltaic performance measurements

The current-voltage characteristics of opaque/transparent devices were performed on the Keithley 2400 digital source under the simulated AM 1.5G (100 mW cm^{-2}) irradiation conditions. The measurements were conducted during R-F scans over a potential range from –0.2 to +1.2 V, divided into 140 points with a scan rate of 10 mV s^{-1} and a delay time of 30 ms, repeated several times until stabilization of the measurement. The EQE curves were collected by Newport Quant X-300, and the light intensity was calibrated using a standard silicon reference detector.

2. Synthesis of BZ-OEG

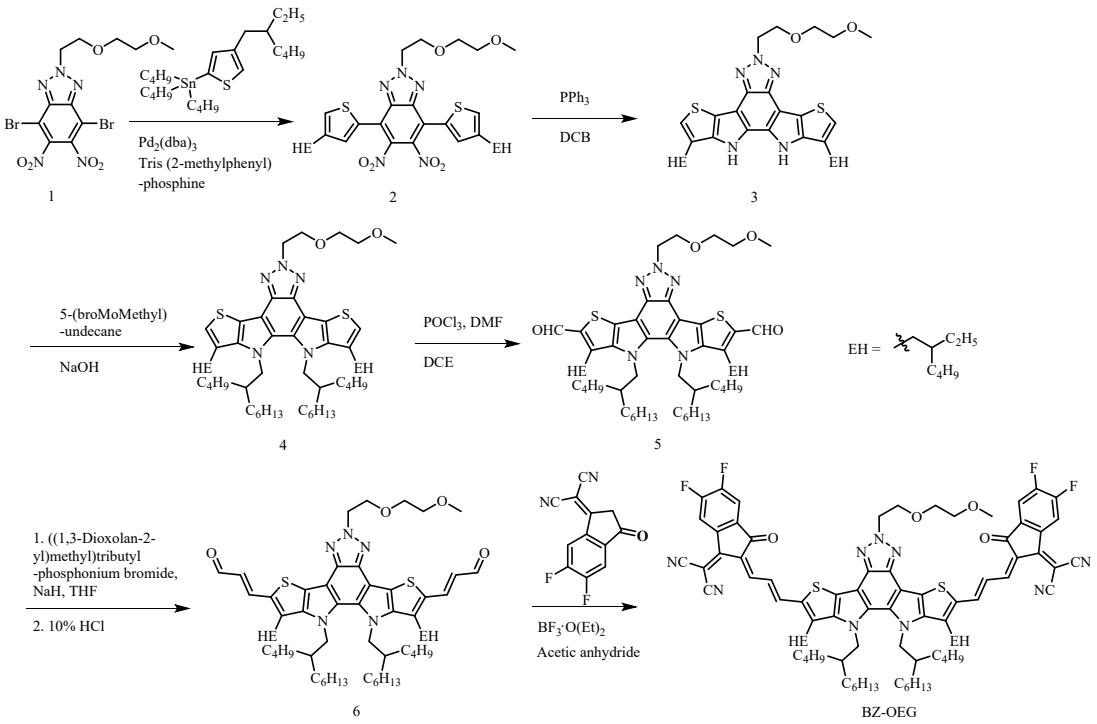

Scheme S1. Synthetic routes of **BZ-OEG**.

Synthesis of 2

1.12 g tributyl(4-(2-ethylhexyl)thiophen-2-yl)stannane (2.3 mmol), 19 mg $Pd_2(dba)_3$ (0.02 mmol), and 25 mg tris (2-methylphenyl)phosphine (0.08 mmol) were added to 10 mL toluene solution of compound 1 (1 mmol). The reaction mixture was then stirred at 90 °C under a nitrogen (N_2) atmosphere for 4 hours. After cooling, the mixture was then extracted with dichloromethane three times. The combined organic layers were concentrated under reduced pressure and purified by silica gel chromatography using hexane/ethyl acetate (3:1, v/v) as the eluent to afford pure compound 2 as yellow liquid (92% yield). ^{1}H NMR (600 MHz, $CDCl_3$) δ = 7.25 – 7.22 (m, 2H), 7.16 – 7.14 (m, 2H), 4.93 (t, *J*=5.6, 2H), 4.14 (t, *J*=5.6, 2H), 3.58 – 3.54 (m, 2H), 3.42 – 3.38 (m, 2H), 3.24 (s, 3H), 2.53 (d, *J*=6.8, 4H), 1.52 – 1.48 (m, 2H), 1.26 – 1.19 (m, 16H), 0.83 (t, *J*=7.4, 12H). ^{13}C NMR (150 MHz, $CDCl_3$) δ = 142.96, 141.76, 139.75, 132.09, 129.15, 126.30, 119.56, 71.83, 70.64, 68.79, 59.04, 57.46, 40.38, 34.27, 32.48, 28.96, 25.60, 23.03,

14.14, 10.86. MALDI-TOF-MS (m/z): calcd for M^+ $C_{35}H_{49}N_5O_6S_2$: 699.3124; found 699.2266.

Synthesis of 3

699 mg compound 2 (1 mmol) and 2.62 g PPh_3 (10 mmol) were dissolved in 6 mL 1,2-dichlorobenzene (DCB). The reaction mixture was then stirred at 180 °C under a nitrogen (N_2) atmosphere for 4 hours. After cooling, removed the solvent of mixtures under vacuum, the crude product of compound 3 was obtained and used in next step without further purification.

Synthesis of 4

Compound 3 (1 mmol), 2 g 5-(broMoMethyl)undecane (8 mmol) and 320 mg NaOH (8 mmol) were dissolved in 10 mL *N*,*N*-dimethylformamide (DMF). The reaction mixture was then stirred at 85 °C under a nitrogen (N_2) atmosphere for 8 hours. After cooling, the mixture was extracted with dichloromethane for three times. The combined organic layers were concentrated under reduced pressure and purified by silica gel chromatography using petroleum ether/ethyl acetate (6:1 v/v) as the eluent to afford pure compound 4 as yellow solid (44% yield). ^{1}H NMR (600 MHz, $CDCl_3$) δ = 6.95 (s, 2H), 5.00 (t, *J*=6.3, 2H), 4.52 – 4.33 (m, 4H), 4.25 (t, *J*=6.2, 2H), 3.66 – 3.59 (m, 2H), 3.51 – 3.47 (m, 2H), 3.33 (s, 3H), 3.01 – 2.64 (m, 4H), 1.92 – 1.82 (m, 2H), 1.76 – 1.69 (m, 2H), 1.55 – 0.16 (m, 72H). ^{13}C NMR (200 MHz, $CDCl_3$) δ = 143.96, 136.25, 133.91, 127.65, 122.28, 122.20, 108.23, 71.87, 70.54, 69.68, 59.03, 55.38, 52.61, 39.63, 38.84, 33.94, 33.14, 32.31, 31.57, 30.54, 29.46, 28.84, 28.50, 26.34, 25.16, 23.09, 22.54, 14.17, 14.01, 13.42, 11.23, 10.70. MALDI-TOF-MS (m/z): calcd for M^+ $C_{59}H_{97}N_5O_2S_2$: 971.7084; found 971.5560.

Synthesis of 5

400 mg compound 4 (0.41 mmol) and 0.35 mL DMF were dissolved in 15 mL dichloroethane (DCE). Under ice bath conditions, 0.38 mL of $POCl_3$ was added and the

mixture was stirred for 40 minutes. The reaction mixture was then stirred at 85 °C under a nitrogen (N_2) atmosphere for 6.5 hours. After cooling, 5 mL saturated K_2CO_3 solution was added, and the mixture was stirred at room temperature for 3 hours. The mixture was then extracted with dichloromethane three times. The combined organic layers were concentrated under reduced pressure and purified by silica gel chromatography using hexane/ethyl acetate (3:1, v/v) as the eluent to afford pure compound 5 as orange liquid (90% yield). ^{1}H NMR (600 MHz, $CDCl_3$) δ = 10.12 (s, 2H), 5.00 (t, *J*=6.0, 2H), 4.54 – 4.39 (m, 4H), 4.26 (t, *J*=6.0, 2H), 3.71 – 3.62 (m, 2H), 3.54 – 3.49 (m, 2H), 3.46 – 3.36 (m, 2H), 3.33 (s, 3H), 3.02 – 2.91 (m, 2H), 1.95 – 1.84 (m, 2H), 1.78 – 1.68 (m, 2H), 1.60 – 0.08 (m, 72H). ^{13}C NMR (125 MHz, $CDCl_3$) δ = 182.35, 144.99, 139.47, 136.92, 136.34, 136.17, 129.45, 110.03, 71.81, 70.50, 69.32, 59.01, 55.61, 52.82, 42.18, 41.41, 38.99, 33.09, 32.39, 31.84, 31.35, 30.56, 29.19, 28.38, 26.17, 25.26, 22.89, 22.33, 14.01, 13.84, 13.30, 11.18, 10.65. MALDI-TOF-MS (m/z): calcd for M^+ $C_{61}H_{97}N_5O_4S_2$: 1027.6982; found 1027.4881.

Synthesis of 6

332 mg ((1,3-Dioxolan-2-yl)methyl)tributylphosphonium bromide (0.90 mmol) was added to 20 mL THF solution of compound 5 (0.35 mmol). Subsequently, 69 mg NaH (60% dispersion in mineral oil) (1.74 mmol) was added to the mixture, and it was stirred at room temperature under a N_2 atmosphere for 16 hours. Then, 3 mL 10% HCl was added, and the mixture was stirred at room temperature for 3 hours. The mixture was then extracted with dichloromethane three times. The combined organic layers were concentrated under reduced pressure and purified by silica gel chromatography using hexane/ethyl acetate (3:1, v/v) as the eluent to afford pure compound 6 as red liquid (76% yield). ^{1}H NMR (500 MHz, $CDCl_3$) δ = 9.68 (d, *J*=7.6, 2H), 7.78 (d, *J*=15.2, 2H), 6.61 (dd, *J*=15.1, 7.5, 2H), 5.01 (t, *J*=5.9, 2H), 4.48 – 4.37 (m, 4H), 4.26 (t, *J*=5.3, 2H), 3.69 – 3.62 (m, 2H), 3.55 – 3.47 (m, 2H), 3.34 (s, 3H), 3.10 – 2.86 (m, 4H), 1.91 – 1.79 (m, 2H), 1.77 – 1.67 (m, 2H), 1.38 – 0.07 (m, 72H). ^{13}C NMR (125 MHz, $CDCl_3$) δ = 192.46, 145.36, 143.71, 136.08, 135.82, 135.25, 132.76, 125.40, 124.92, 109.48, 71.82, 70.51, 69.43, 59.01, 55.60, 52.66, 41.63, 41.01, 38.92, 33.16, 32.03, 31.45, 30.52,

29.65, 29.28, 28.33, 26.27, 25.19, 22.88, 22.39, 14.02, 13.85, 13.31, 11.32, 10.78. MALDI-TOF-MS (m/z): calcd for M^+ $C_{65}H_{101}N_5O_4S_2$: 1079.7275; found 1079.5651.

Synthesis of BZ-OEG

170 mg compound 6 (0.16 mmol), 109 mg 5,6-difluoro-3-(dicyanomethylidene)-1-one (0.47 mmol), 0.2 mL acetic anhydride, and 0.2 mL $BF_3{\cdot}O(Et)_2$ were dissolved in 10 mL toluene. The mixture was then stirred at room temperature for 2 hours. After the reaction was completed, the mixture was extracted with dichloromethane and the combined organic layers were concentrated under reduced pressure. The crude product was purified by silica gel chromatography using chloroform/tetrahydrofuran (110:1, v/v) as the eluent to afford pure compound BZ-OEG as a black solid (81% yield). ^{1}H NMR (600 MHz, $CDCl_3$) δ = 8.76 – 8.69 (m, 2H), 8.56 – 8.47 (m, 4H), 7.75 (d, *J*=14.3, 2H), 7.68 (t, *J*=7.4, 2H), 5.04 (t, *J*=6.0, 2H), 4.50 – 4.36 (m, 4H), 4.35 – 4.28 (m, 2H), 3.77 – 3.68 (m, 2H), 3.59 – 3.52 (m, 2H), 3.37 (s, 3H), 3.13 – 3.01 (m, 2H), 3.00 – 2.88 (m, 2H), 1.89 – 1.78 (m, 2H), 1.77 – 1.70 (m, 2H), 1.59 – 1.17 (m, 36H), 1.06 – 0.77 (m, 20H), 0.68 – 0.14 (m, 16H). ^{13}C NMR (150 MHz, $CDCl_3$) δ = 186.94, 157.66, 155.20, 153.46, 146.85, 145.39, 140.33, 136.50, 136.22, 135.29, 134.95, 129.42, 123.12, 122.46, 114.85, 114.62, 112.55, 110.95, 71.88, 70.60, 69.33, 59.11, 55.79, 53.04, 42.21, 41.69, 39.03, 33.30, 32.29, 31.47, 30.57, 29.52, 29.30, 28.54, 26.38, 25.50, 22.92, 22.43, 14.16, 13.89, 13.41, 11.48, 10.93. MALDI-TOF-MS (m/z): calcd for M^+ $C_{89}H_{105}F_4N_9O_4S_2$: 1503.7667; found 1503.5523.

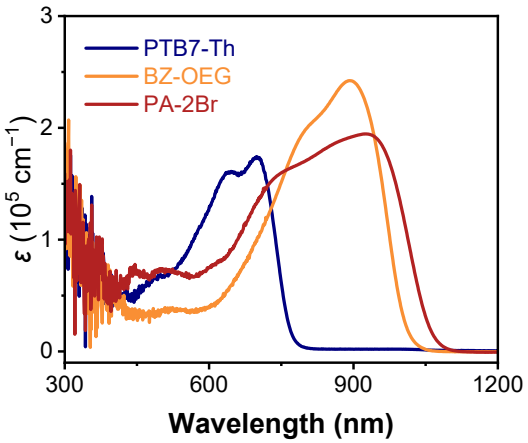

Figure S1. Absorption coefficient spectra of PTB7-Th, BZ-OEG, and PA-2Br films.

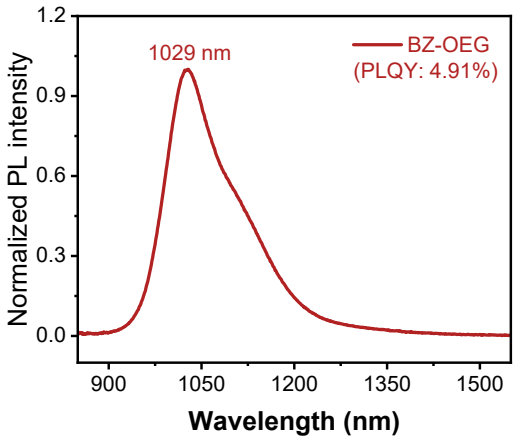

Figure S2. PL spectrum of BZ-OEG film.

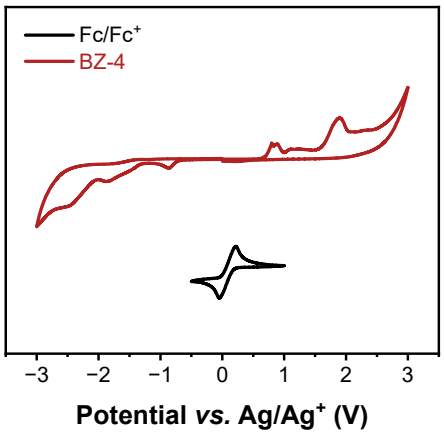

Figure S3. Cyclic voltammogram of BZ-OEG neat film.

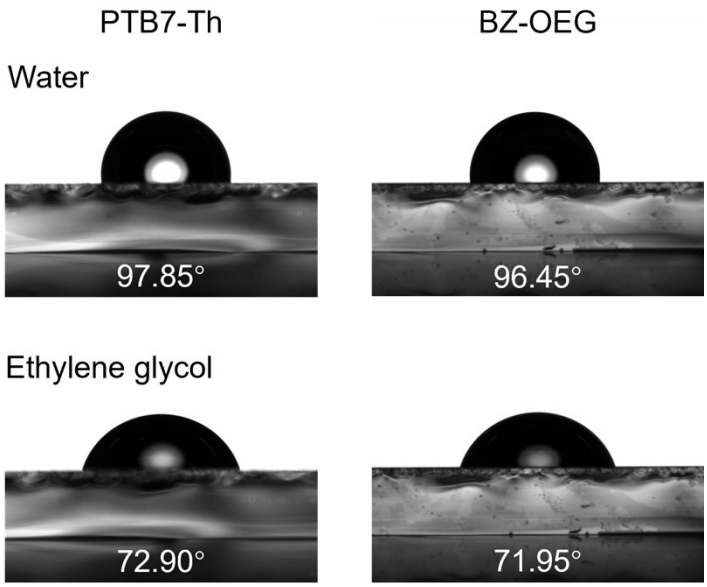

Figure S4. Contact angle measurements of water and ethylene glycol droplets atop the surfaces of neat PTB7-Th and BZ-OEG films.

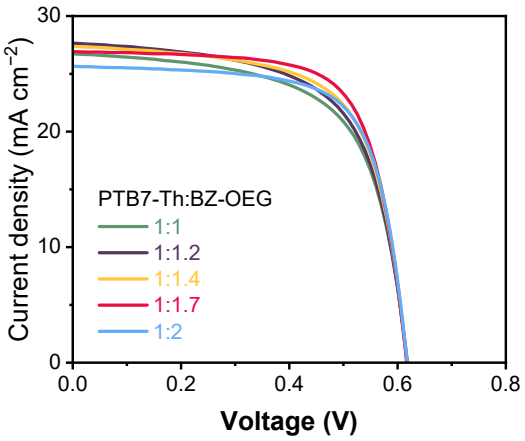

Figure S5. *J-V* curves of PTB7-Th:BZ-OEG-based opaque devices with different D/A ratios.

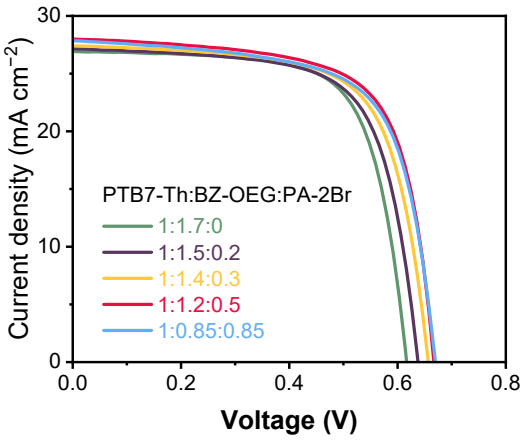

Figure S6. *J-V* curves of PTB7-Th:BZ-OEG:PA-2Br-based opaque devices with various PA-2Br contents.

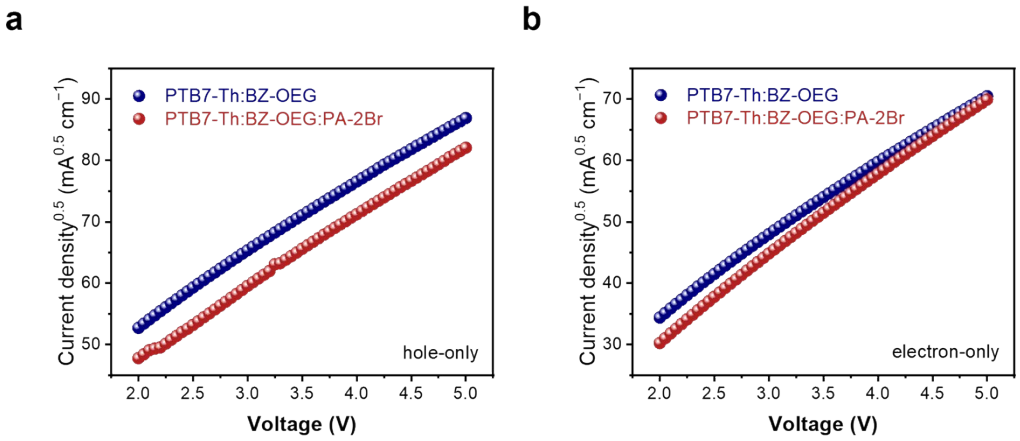

Figure S7. Mobilities measurement plots of (a) hole-only and (b) electron-only devices based on binary and ternary active layer.

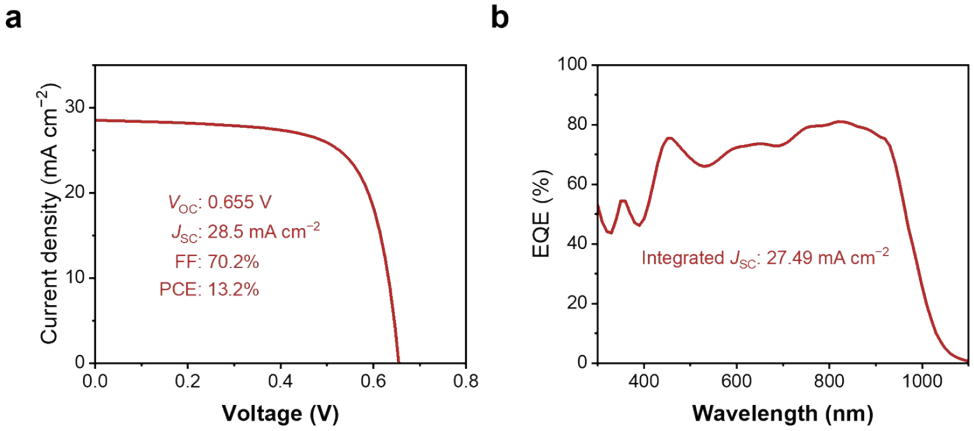

Figure S8. (a) *J-V* curve and (b) EQE curve of optimized ternary OPVs.

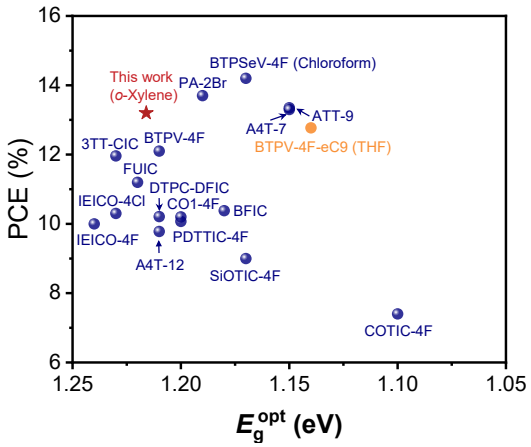

Figure S9. Summary of efficient OPVs employing ultra-narrow-bandgap acceptors with *E*opt g below 1.25 eV.

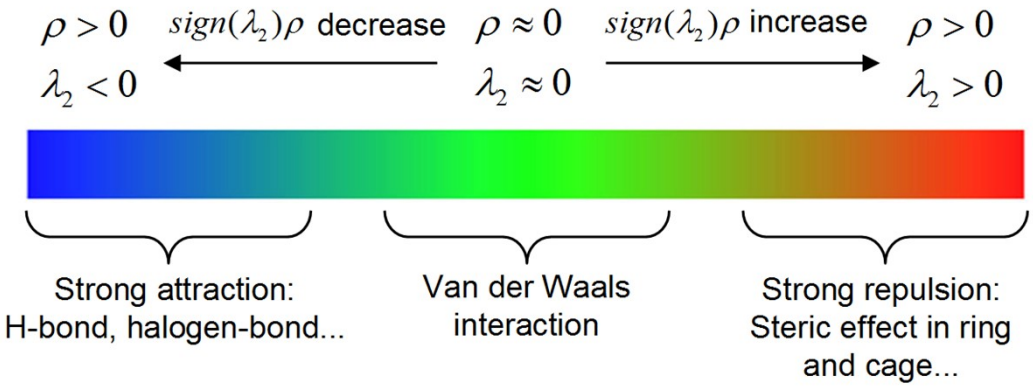

Figure S10. The color bar indicates the $sign(\lambda_2)\rho$ values, with blue representing prominent attractive interactions, red indicating prominent repulsive interactions in the regions with steric effect, and green exhibiting very weak interactions.

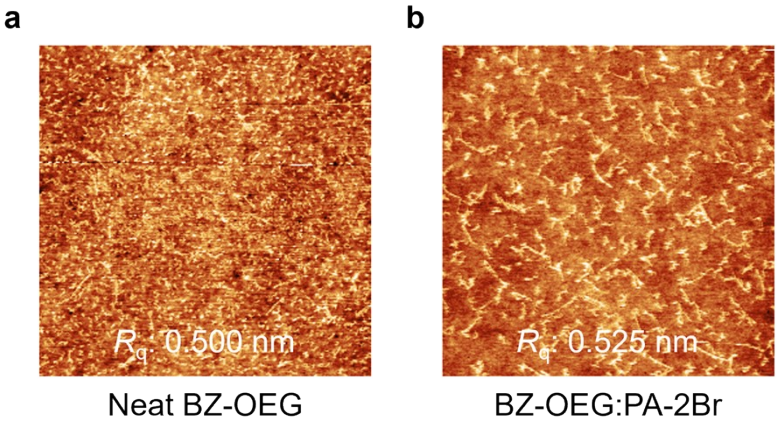

Figure S11. AFM images of (a) neat BZ-OEG film and (b) BZ-OEG:PA-2Br blend film.

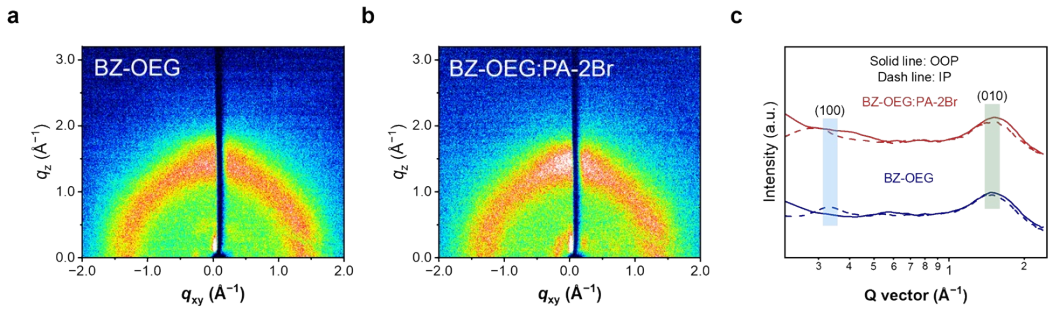

Figure S12. 2D GIWAXS patterns and their corresponding 1D line-cut profiles of neat BZ-OEG film and BZ-OEG:PA-2Br blend film.

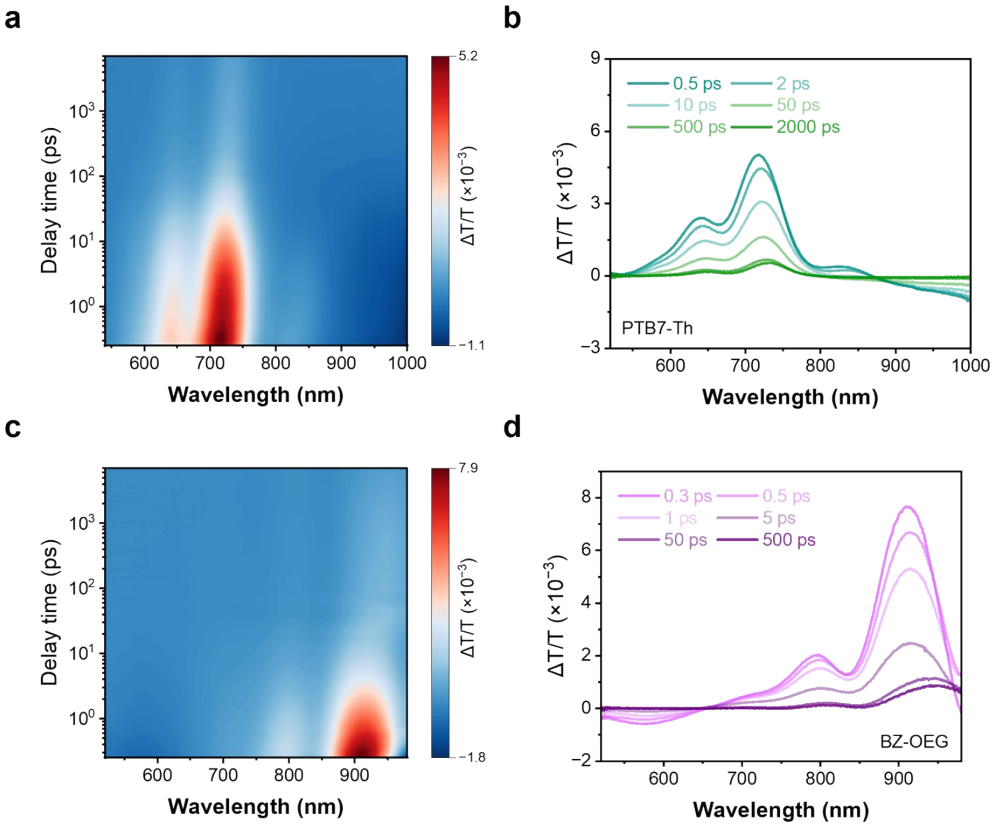

Figure S12. Color plot of the TA spectra and representative spectra at various delay times for (a, b) PTB7-T film (under 500 nm excitation) and (c, d) BZ-OEG film (under 900 nm excitation) in VIS-NIR region.

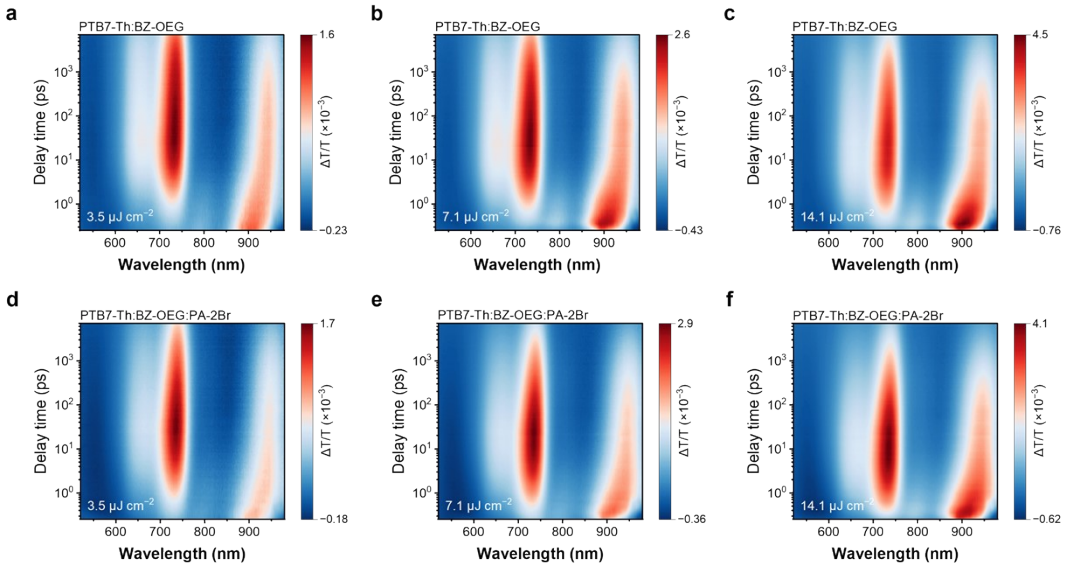

Figure S13. 2D contour maps of TA spectra under different excitation intensity for (a-c) PTB7-Th:BZ-OEG blend and (d-f) PTB7-Th:BZ-OEG:PA-2Br blend films, respectively (under 900 nm excitation).

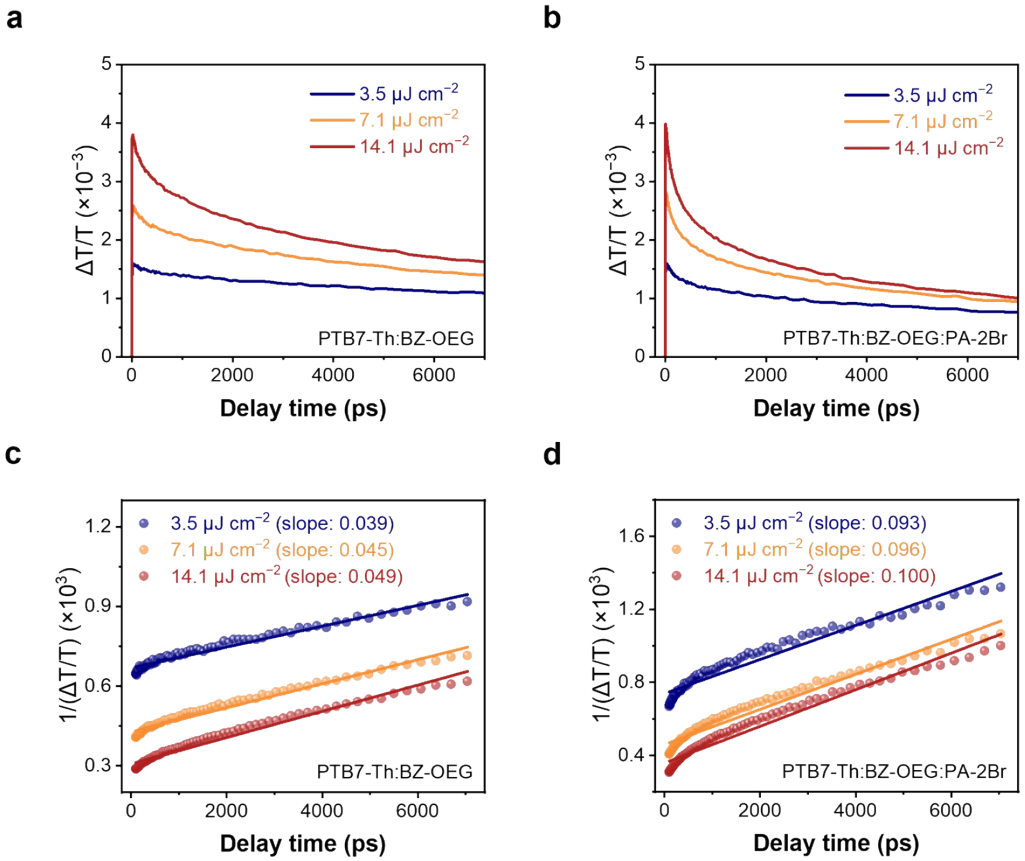

Figure S14. Decay kinetics probing at 730 nm under different excitation intensities for (a, c) PTB7-Th:BZ-OEG blend and (b, d) PTB7-Th:BZ-OEG:PA-2Br blend films, respectively.

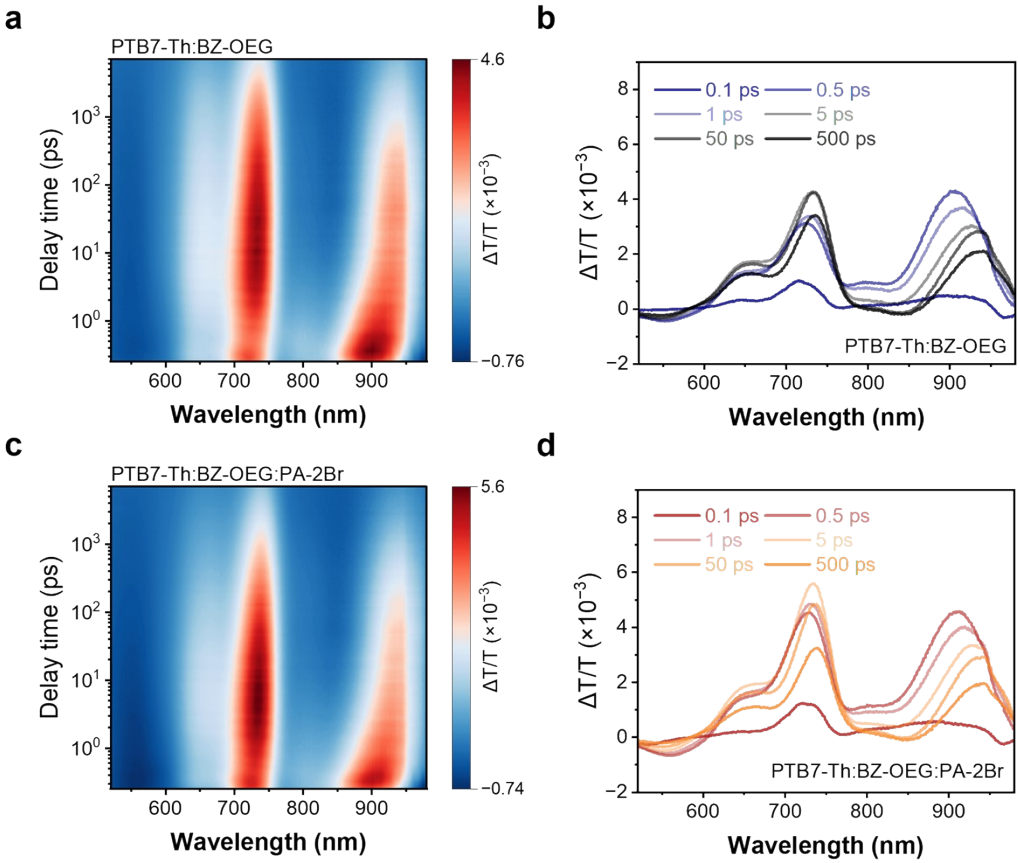

Figure S15. Color plot of the TA spectra and representative spectra at various delay times for (a, b) PTB7-Th:BZ-OEG blend and (c, d) PTB7-Th:BZ-OEG:PA-2Br blend films (under 500 nm excitation) in VIS-NIR region.

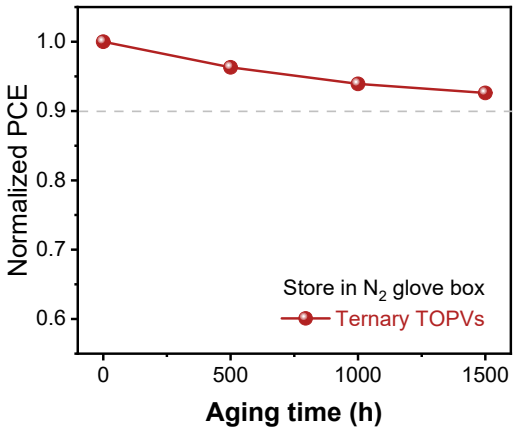

Figure S16. Efficiency decay of PTB7-Th:BZ-OEG:PA-2Br-based TOPVs under shelf-storage.

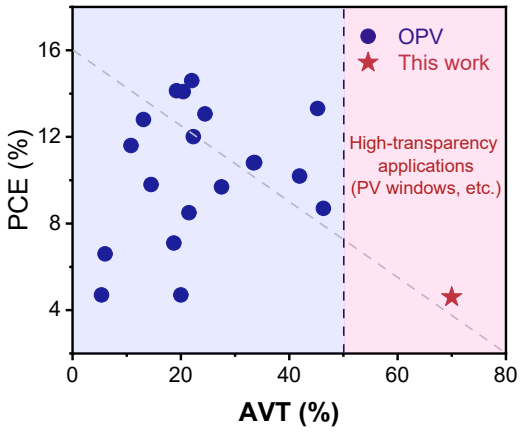

Figure S17. Summary of TOPVs processed by non-halogenated solvents.

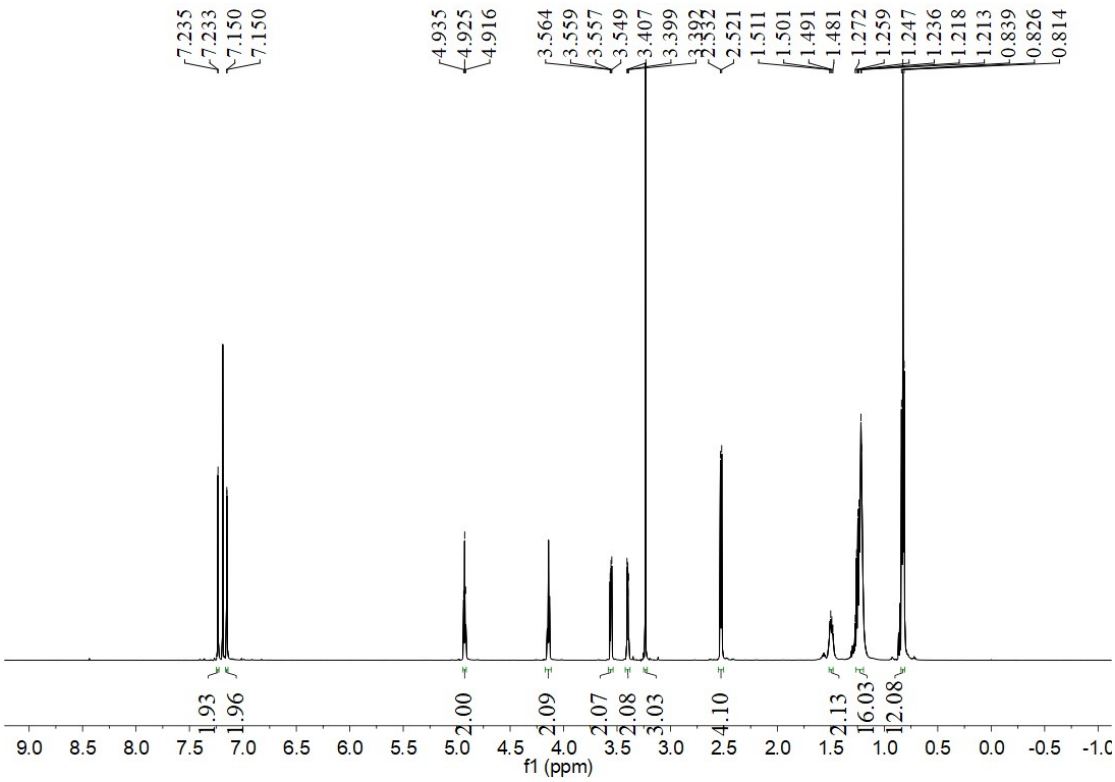

Figure S18. ^{1}H NMR spectrum of compound 2.

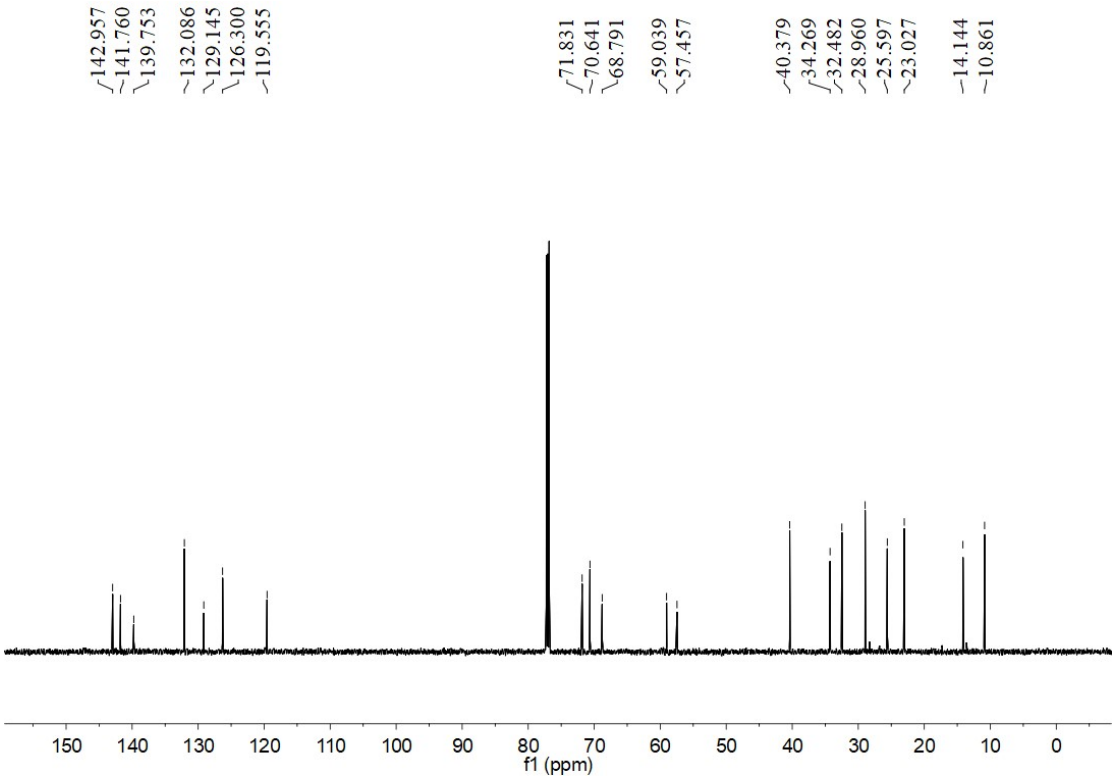

Figure S19. ^{13}C NMR spectrum of compound 2.

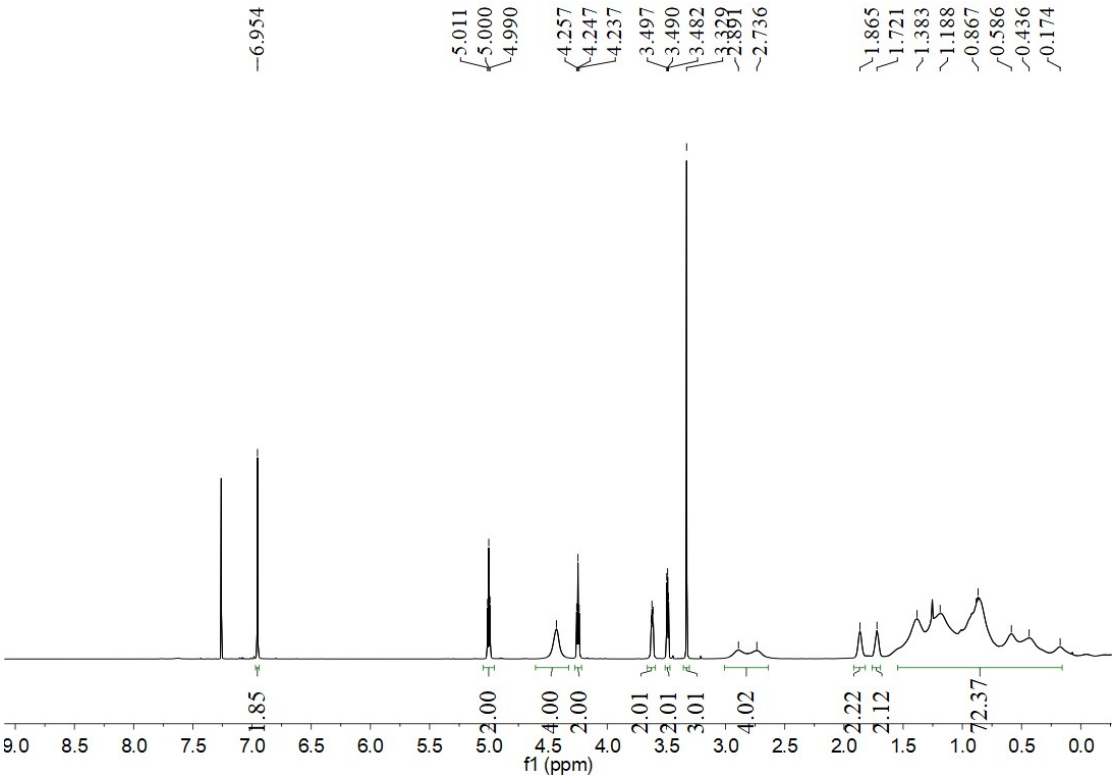

Figure S20. ^{1}H NMR spectrum of compound 4.

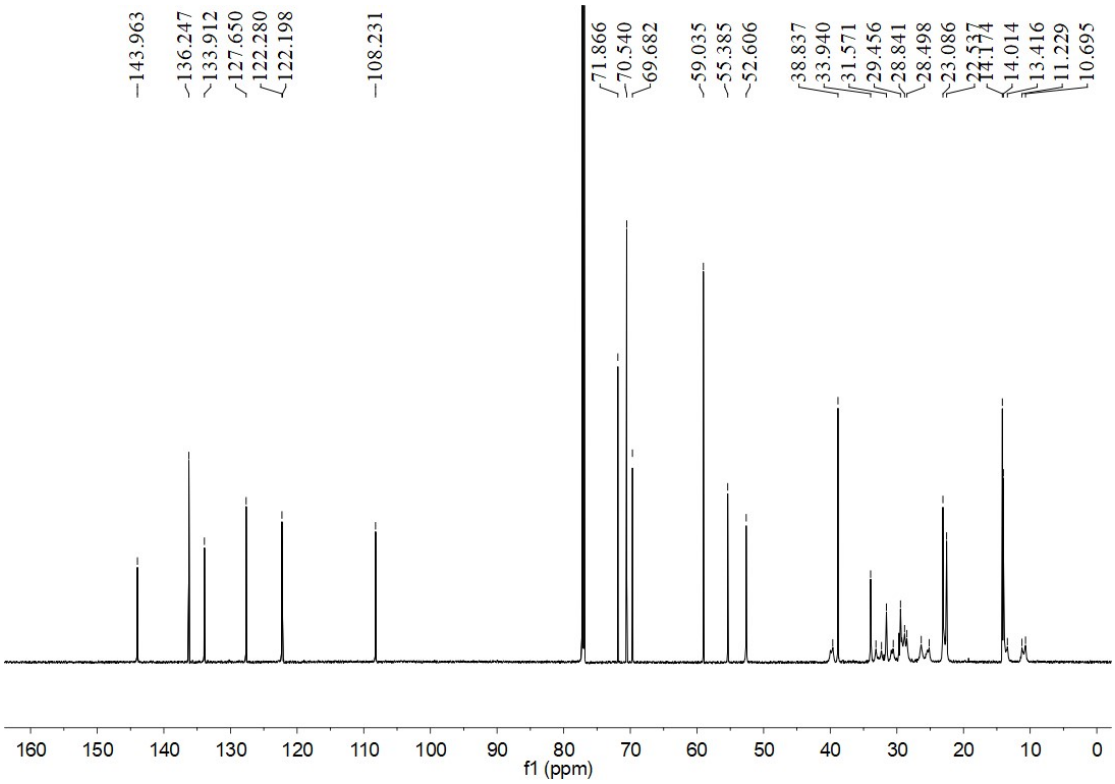

Figure S21. ^{13}C NMR spectrum of compound 4.

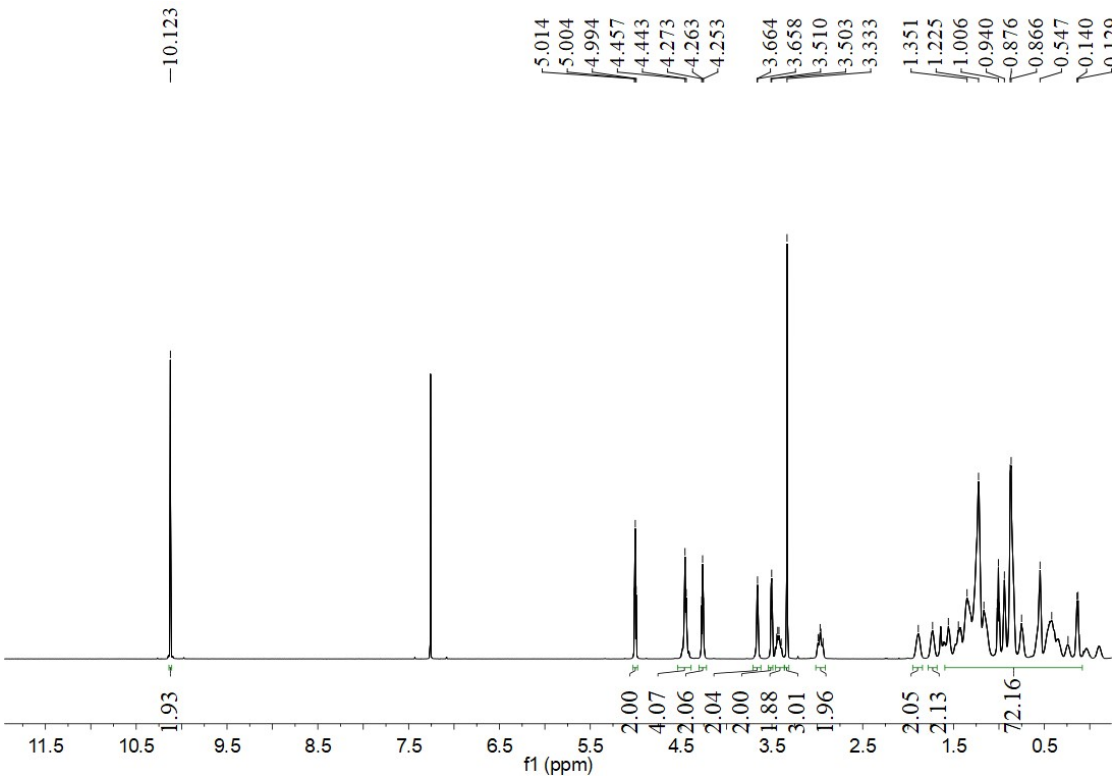

Figure S22. ^{1}H NMR spectrum of compound 5.

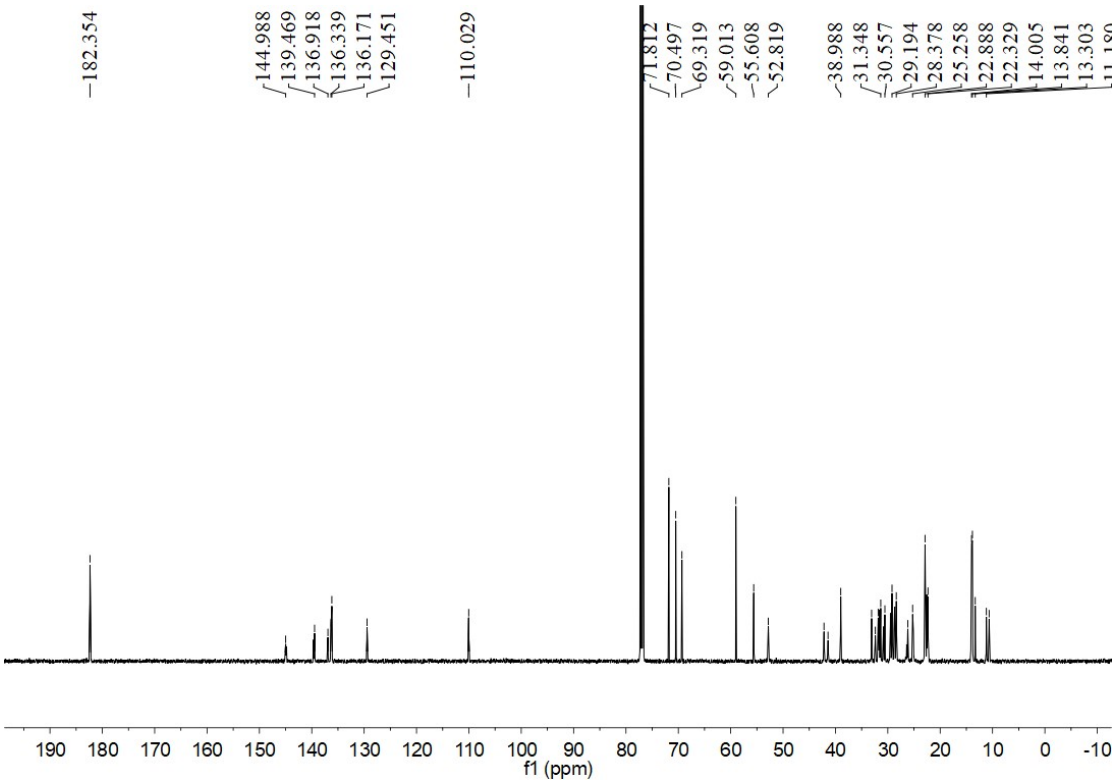

Figure S23. ^{13}C NMR spectrum of compound 5.

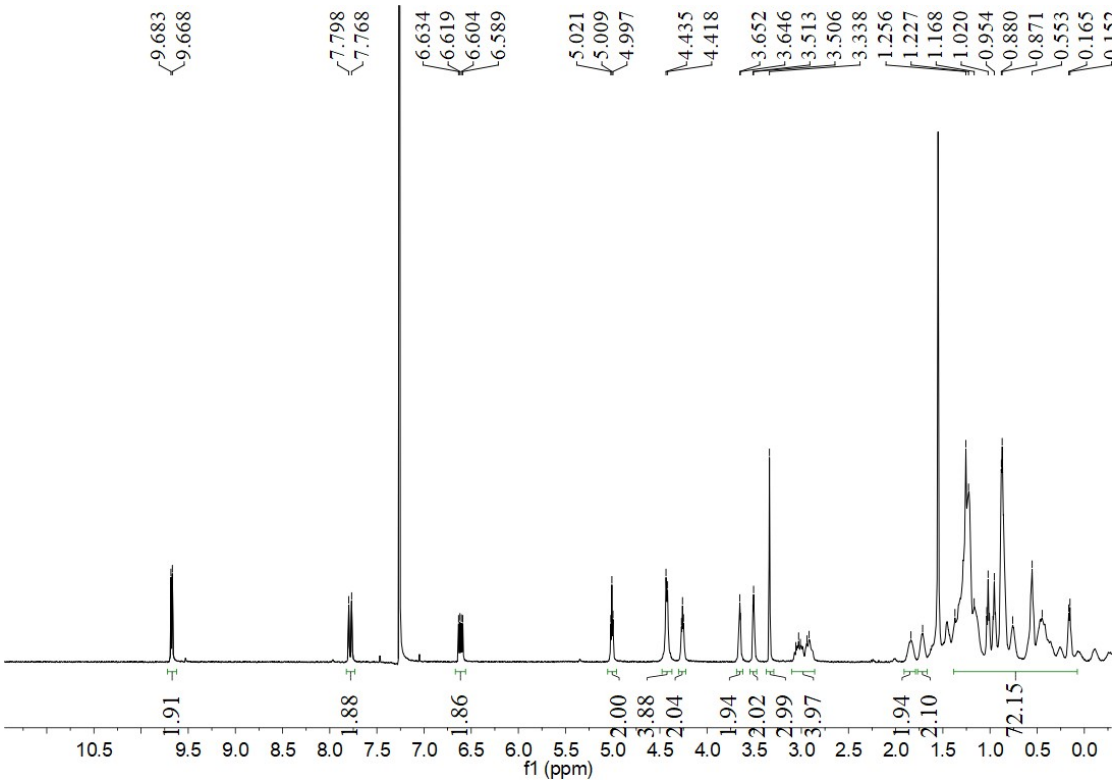

Figure S24. ^{1}H NMR spectrum of compound 6.

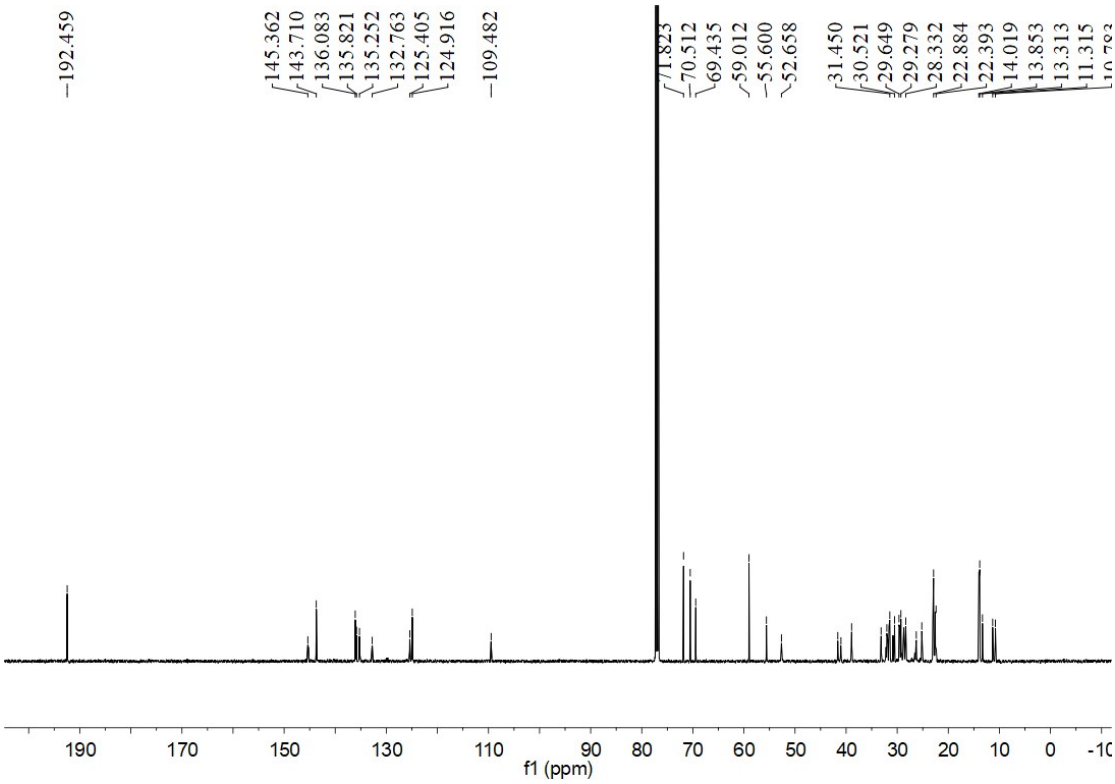

Figure S25. ^{13}C NMR spectrum of compound 6.

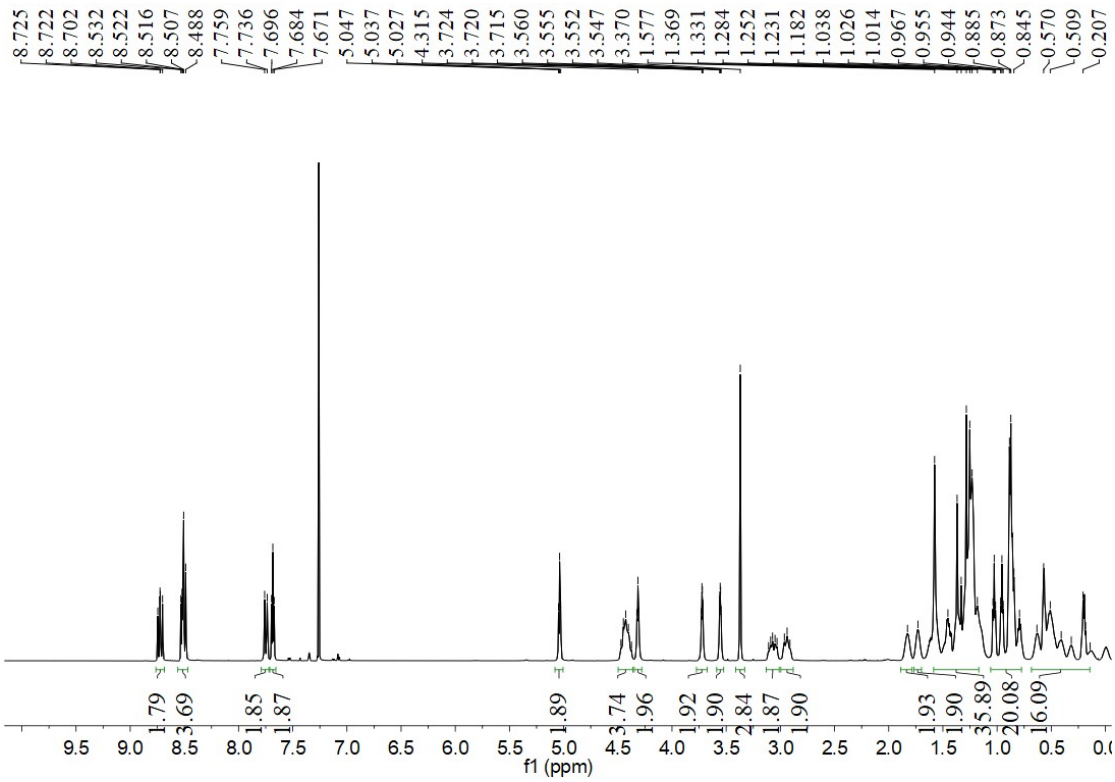

Figure S26. ^{1}H NMR spectrum of BZ-OEG.

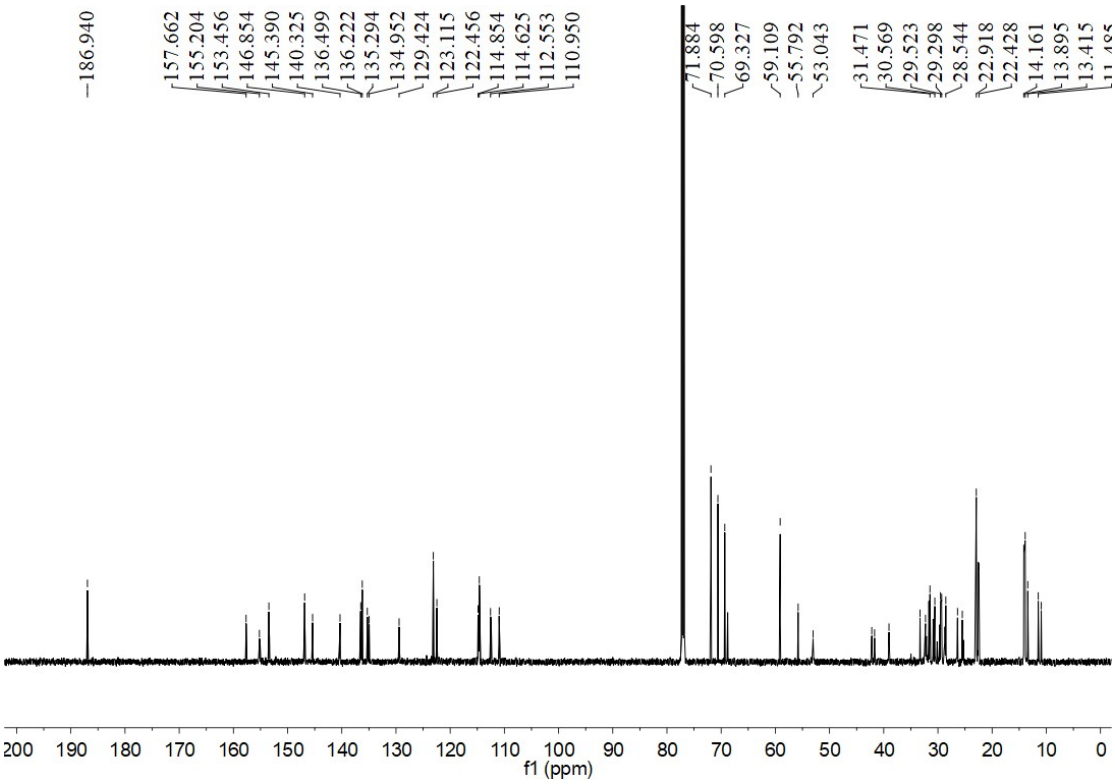

Figure S27. ^{13}C NMR spectrum of BZ-OEG.

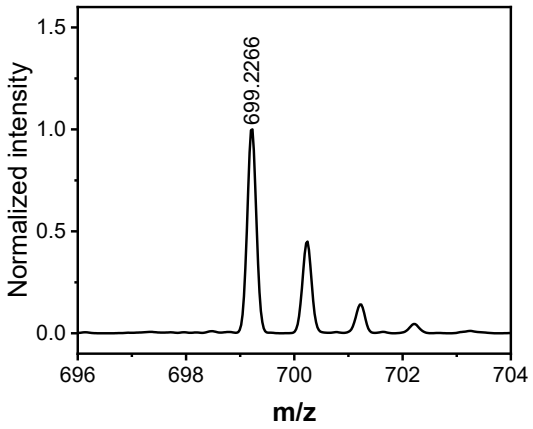

Figure S28. MALDI-TOF spectra of compound 2.

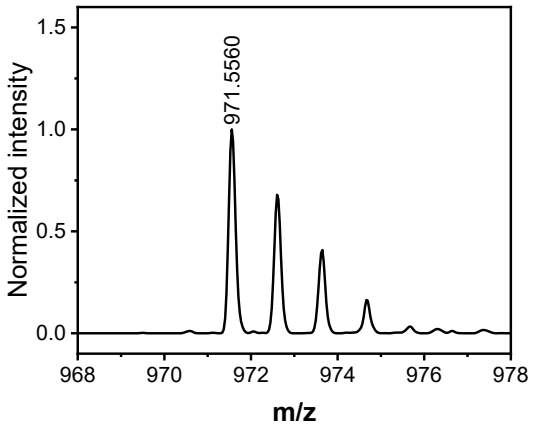

Figure S29. MALDI-TOF spectra of compound 4.

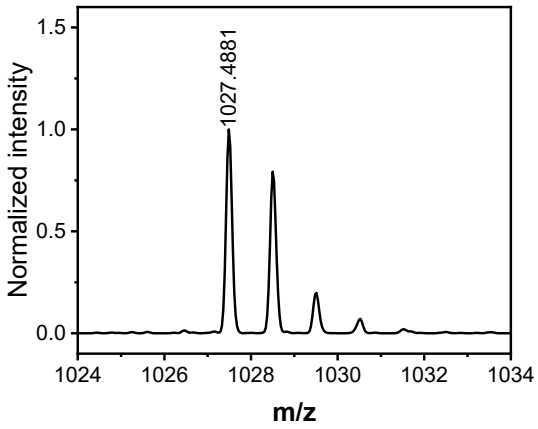

Figure S30. MALDI-TOF spectra of compound 5.

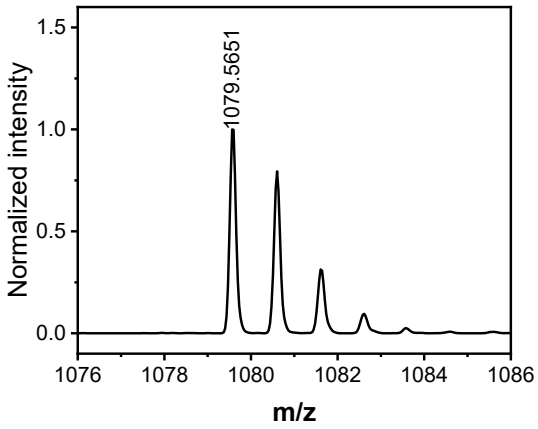

Figure S31. MALDI-TOF spectra of compound 6.

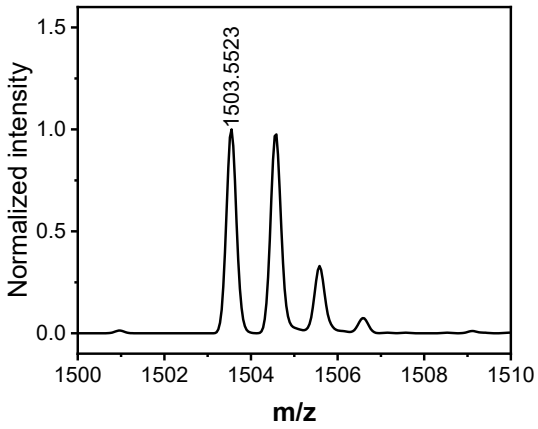

Figure S32. MALDI-TOF spectra of BZ-OEG.

Table S1. Photophysical properties of BZ-OEG.

Acceptor	**λsol max (nm)**	**λsol onset (nm)**	**λfilm max (nm)**	**λfilm onset (nm)**	***E*opt g[(a)](eV)**
BZ-OEG	779	835	893	1007	1.231

[(a)] Optical bandgap calculated from the absorption edge of the film using the formula: Eopt g=1240/λ_{onset}.

Table S2. The energy levels of BZ-OEG obtained from CV.

Sample	E_{ox} (V)	E_{red} (V)	HOMO (eV)	LUMO (eV)	$E_{cv\ g}$ (eV)
Fc/Fc^{+}	−0.016	0.191	-	-	-
BZ-OEG	0.678	−0.718	−5.49	−3.89	1.60

Table S3. Detailed photovoltaic parameters of PTB7-Th:BZ-OEG-based opaque devices with different D/A ratios.

PTB7-Th:BZ-OEG	V_{OC} (V)	J_{SC} (mA cm^{-2})	FF (%)	PCE (%)
1:1	0.618	26.7	63.5	10.5
1:1.2	0.617	27.6	63.6	10.8
1:1.4	0.617	27.3	66.2	11.2
1:1.7	0.617	26.9	70.2	11.7
1:2	0.617	25.6	70.1	11.1

Table S4. Detailed photovoltaic parameters of PTB7-Th:BZ-OEG:PA-2Br-based opaque devices with various PA-2Br contents.

PTB7-Th:BZ-OEG:PA-2Br	V_{OC} (V)	J_{SC} (mA cm^{-2})	FF (%)	PCE (%)
1:1.7:0	0.617	26.9	70.2	11.7
1:1.5:0.2	0.637	27.1	68.6	11.9
1:1.4:0.3	0.657	27.4	68.3	12.3
1:1.2:0.5	0.667	28.0	68.4	12.8
1:0.85:0.85	0.669	27.8	67.3	12.5

Table S5. Summary of reported data shown in Figure S9.

Ref.	Donor:Acceptor	Processing solvent	λ_{onset} (nm)	*E*opt g(eV)	PCE (%)	Year
[3]	PTB7-Th:IEICO-4F	Chloroform	1000	1.24	10.0	2017
[4]	PTB7-Th:IEICO-4Cl		1008	1.23	10.3	2017
[5]	PTB7-Th:3TT-CIC		1008	1.23	11.96	2019
[6]	PTB7-Th:FUIC		1016	1.22	11.2	2019
[7]	PTB7-Th:A4T-12		1025	1.21	9.78	2024
[8]	PTB7-Th:DTPC-DFIC		1025	1.21	10.21	2018
[9]	PTB7-Th:BTPV-4F		1025	1.21	12.1	2021
[10]	PM6:PDTTIC-4F		1033	1.20	10.07	2021
[11]	PTB7-Th:CO1-4F		1033	1.20	10.2	2019
[12]	PTB7-Th:PA-2Br		1042	1.19	13.7	2025
[13]	PTB7-Th:BFIC		1051	1.18	10.38	2022
[14]	PTB7-Th:SiOTIC-4F		1060	1.17	9.0	2018
[15]	PTB7-Th:BTPSeV-4F		1060	1.17	14.2	2023
[7]	PTB7-Th:A4T-7		1078	1.15	13.3	2024
[16]	PTB7-Th:ATT-9		1078	1.15	13.35	2022
[14]	PTB7-Th:COTIC-4F		1127	1.10	7.4	2018
[17]	PTB7-Th:BTPV-4F-eC9	Tetrahydrofuran	1088	1.14	12.77	2021
This work	**PTB7-Th:BZ-OEG:PA-2Br**	***o*-Xylene**	**1020**	**1.22**	**13.2**	**2025**

Table S6. Energy loss analysis of the binary and ternary OPVs.

active layer	E_g (eV)	E_{loss} (eV)	ΔE_1 (eV)	ΔE_2 (eV)	$\Delta E_{3(cal.)}$ (eV)	$\Delta E_{3(exp.)}$ (eV)
PTB7-Th:BZ-OEG	1.268	0.651	0.256	0.070	0.322	0.325
PTB7-Th:BZ-OEG:PA-2Br	1.252	0.585	0.252	0.045	0.284	0.288

Table S7. The detailed parameters about *d*-spacings and CCLs of BZ-OEG neat films and BZ-OEG:PA-2Br blend films based on their corresponding 2D GIWAXS.

Acceptor films	Direction	*q* (Å^{-1})	*d*-spacing (Å)	FWHM (Å^{-1})	CCL (Å)
BZ-OEG	OOP	1.453	4.324	0.528	10.710
	IP	0.310	20.268	0.081	69.813
BZ-OEG:PA-2Br	OOP	1.467	4.283	0.516	10.959
	IP	0.288	21.817	0.072	78.540

Table S8. The detailed parameters about *d*-spacings and CCLs of PTB7-Th:BZ-OEG and PTB7-Th:BZ-OEG:PA-2Br blend films based on their corresponding 2D GIWAXS.

active layer films	Direction	*q* (Å^{-1})	*d*-spacing (Å)	FWHM (Å^{-1})	CCL (Å)
PTB7-Th:BZ-OEG	OOP	1.504	4.178	0.568	9.956
	IP	0.334	18.812	0.108	52.360
PTB7-Th:BZ-OEG:PA-2Br	OOP	1.540	4.080	0.560	10.098
	IP	0.309	20.334	0.100	56.549

Table S9. Summary of the reported nonhalogenated-solvent-processed TOPVs.

Ref.	Absorption layer	Active area (cm^2)	AVT (%)	PCE (%)	LUE (%)	CRI	Year
[18]	P3HT:IDTBR	59.52	5.35	4.7	0.251	-	2018
[19]	PffBT4T-2OD:$PC_{61}BM$:$PC_{71}BM$	≤0.1	6	6.6	0.396	-	2016
[20]	PM6:DTY6	18	10.8	11.6	1.25	-	2020
[21]	PM6:L8-BO	18.73	13.1	12.80	1.68		2025
[20]	PM6:DTY6	18	14.5	9.8	1.42	-	2020
[20]	PM6:DTY6	18	18.7	7.1	1.33	-	2020
[22]	PBDB-TF:BTIC-2Cl-γCF_3:PC_{71}ThBM	0.04	19.20	14.13	2.71	-	2020
[23]	PBTZT-stat-BDTT-8:4TICO	0.08	20	4.7	0.940	-	2020
[24]	PM6-Ir1:BTP-eC9:$PC_{71}BM$	0.05	20.44	14.09	2.88	96.5	2022
[25]	PTB7-Th/IEICO-4F	0.04	21.5	8.5	1.83	59.87	2020
[26]	DEH-20:L8-BO	0.043	22	14.6	3.21	-	2022
[27]	PM6:BTP-BO-4Cl	18.73	22.3	12.01	2.68	-	2022
[22]	PBDB-TF:BTIC-2Cl-γCF_3:PC_{71}ThBM	0.04	24.45	13.06	3.19	-	2020
[28]	PM6:CH7	25.2	27.5	9.69	2.66	-	2023
[29]	PM7/BTP-eC9	0.04	33.4	10.8	3.61	74.48	2022
[22]	PBDB-TF:BTIC-2Cl-γCF_3:PC_{71}ThBM	0.04	33.61	10.82	3.64	-	2020
[30]	PCE10:eC9-2Cl	0.0484	41.9	10.19	4.27	61	2025
[31]	D18:BTP-eC9:BTO-BO	0.0628	45.23	13.31	6.02	-	2025
[32]	PV2300:PV-A-3:N1100	0.0925	46.3	8.7	4.03	-	2022
This work	**PTB7-Th:BZ-OEG:PA-2Br**	**0.03**	**70.0**	**4.60**	**3.22**	**87.8**	**2025**

Reference

[1] D. Liu, T. L. Kelly, *Nature Photonics* **2013**, 8, 133.

[2] X. Song, K. Zhang, R. Guo, K. Sun, Z. Zhou, S. Huang, L. Huber, M. Reus, J. Zhou, M. Schwartzkopf, S. V. Roth, W. Liu, Y. Liu, W. Zhu, P. Müller-Buschbaum, *Advanced Materials* **2022**, 34, 2200907.

[3] H. Yao, Y. Cui, R. Yu, B. Gao, H. Zhang, J. Hou, *Angewandte chemie international edition* **2017**, 56, 3045.

[4] Y. Cui, C. Yang, H. Yao, J. Zhu, Y. Wang, G. Jia, F. Gao, J. Hou, *Advanced Materials* **2017**, 29, 1703080.

[5] H. H. Gao, Y. Sun, Y. Cai, X. Wan, L. Meng, X. Ke, S. Li, Y. Zhang, R. Xia, N. Zheng, Z. Xie, C. Li, M. Zhang, H. L. Yip, Y. Cao, Y. Chen, *Advanced Energy Materials* **2019**, 9, 1901024.

[6] T. Li, L. Yang, Y. Xiao, K. Liu, J. Wang, X. Lu, X. Zhan, *Journal of Materials Chemistry A* **2019**, 7, 20667.

[7] L. Ma, S. Zhang, J. Zhu, Z. Chen, T. Zhang, X. Hao, J. Hou, *Joule* **2024**, 8, 2238.

[8] Z. Yao, X. Liao, K. Gao, F. Lin, X. Xu, X. Shi, L. Zuo, F. Liu, Y. Chen, A. K. Y. Jen, *Journal of the American Chemical Society* **2018**, 140, 2054.

[9] Z. Jia, S. Qin, L. Meng, Q. Ma, I. Angunawela, J. Zhang, X. Li, Y. He, W. Lai, N. Li, H. Ade, C. J. Brabec, Y. Li, *Nature Communications* **2021**, 12, 178.

[10] Y. Chen, Y. Zheng, Y. Jiang, H. Fan, X. Zhu, *Journal of the American Chemical Society* **2021**, 143, 4281.

[11] J. Lee, S.-J. Ko, H. Lee, J. Huang, Z. Zhu, M. Seifrid, J. Vollbrecht, V. V. Brus, A. Karki, H. Wang, K. Cho, T.-Q. Nguyen, G. C. Bazan, *ACS Energy Letters* **2019**, 4, 1401.

[12] Y. Zhou, Z. Zhou, Y. Wang, Q. Jiang, D. Liu, *Small* **2025**, 21, 500536.

[13] Y. Zhang, Q. Wei, Z. He, Y. Wang, T. Shan, Y. Fu, X. Guo, H. Zhong, *ACS Applied Materials & Interfaces* **2022**, 14, 31066.

[14] J. Lee, S. J. Ko, M. Seifrid, H. Lee, B. R. Luginbuhl, A. Karki, M. Ford, K. Rosenthal, K. Cho, T. Q. Nguyen, G. C. Bazan, *Advanced Energy Materials* **2018**, 8,

1801212.

[15] Z. Jia, Q. Ma, Z. Chen, L. Meng, N. Jain, I. Angunawela, S. Qin, X. Kong, X. Li, Y. Yang, H. Zhu, H. Ade, F. Gao, Y. Li, *Nature Communications* **2023**, 14, 1236.

[16] W. Liu, S. Sun, S. Xu, H. Zhang, Y. Zheng, Z. Wei, X. Zhu, *Advanced Materials* **2022**, 34, 2200337.

[17] S. Qin, Z. Jia, L. Meng, C. Zhu, W. Lai, J. Zhang, W. Huang, C. Sun, B. Qiu, Y. Li, *Advanced Functional Materials* **2021**, 31, 2102361.

[18] S. Strohm, F. Machui, S. Langner, P. Kubis, N. Gasparini, M. Salvador, I. McCulloch, H. J. Egelhaaf, C. J. Brabec, *Energy & Environmental Science* **2018**, 11, 2225.

[19] J. Czolk, D. Landerer, M. Koppitz, D. Nass, A. Colsmann, *Advanced Materials Technologies* **2016**, 1, 1600184.

[20] S. Dong, T. Jia, K. Zhang, J. Jing, F. Huang, *Joule* **2020**, 4, 2004.

[21] J. Y. Fan, Z. X. Liu, H. Chen, C. Z. Li, *Advanced Materials* **2025**, 37, 2419525.

[22] H. Chen, H. Lai, Z. Chen, Y. Zhu, H. Wang, L. Han, Y. Zhang, F. He, *Angewandte Chemie International Edition* **2020**, 60, 3238.

[23] E. Pascual-San-José, G. Sadoughi, L. Lucera, M. Stella, E. Martínez-Ferrero, G. E. Morse, M. Campoy-Quiles, I. Burgués-Ceballos, *Journal of Materials Chemistry A* **2020**, 8, 9882.

[24] X. Yuan, R. Sun, Y. Wu, T. Wang, Y. Wang, W. Wang, Y. Yu, J. Guo, Q. Wu, J. Min, *Advanced Functional Materials* **2022**, 32, 2200107.

[25] Y. Song, K. Zhang, S. Dong, R. Xia, F. Huang, Y. Cao, *ACS Applied Materials & Interfaces* **2020**, 12, 18473.

[26] Y. Luo, X. Wang, M. Zhang, X. Sun, A. Saparbaev, S. Lei, J. Zhang, B. Xiao, C. Yang, Z. Liu, R. Yang, *Solar RRL* **2022**, 6, 2200679.

[27] J. Y. Fan, Z. X. Liu, J. Rao, K. Yan, Z. Chen, Y. Ran, B. Yan, J. Yao, G. Lu, H. Zhu, C. Z. Li, H. Chen, *Advanced Materials* **2022**, 34, 2110569.

[28] S. Zhang, H. Chen, P. Wang, S. Li, Z. Li, Y. Huang, J. Liu, Z. Yao, C. Li, X. Wan, Y. Chen, *Solar RRL* **2023**, 7, 2300029.

[29] S. J. Jeon, N. G. Yang, Y. H. Kim, J. H. Yun, D. K. Moon, *ACS Applied Materials*

& Interfaces **2022**, 14, 38031.

[30] C. Han, Z. Jin, C. Shen, M. Liu, W. Song, Q. Liu, Z. Ge, *Advanced Energy Materials* **2025**, 15, 2501682.

[31] J. Ding, H. Mou, H. Chen, J. Xu, W. Sun, J. Zhu, Y. Wang, Y. Huang, Y. Li, Y. Li, *Advanced Materials* **2025**, 37, 2420439.

[32] L. Pap, B. Schirmacher, E. Bloch, S. Bogati, P. Viehmann, A. Scheel, D. Müller, M. List, B. Zimmermann, U. Würfel, *Solar RRL* **2023**, 7, 2300561.